

Use of low-density foams as pressure amplifiers in equation-of-state experiments with laser-driven shock waves

Dimitri Batani,¹ Antonio Balducci,¹ Wigen Nazarov,² Thorsten Löwer,³ Tom Hall,⁴ Michel Koenig,⁵ Bernard Faral,⁵ Alessandra Benuzzi,⁵ and Mauro Temporal⁵

¹*Dipartimento di Fisica "G. Occhialini," Università di Milano-Bicocca and INFN, Via Emanueli, 15, 20126 Milano, Italy*

²*Department of Chemistry, University of Dundee, Dundee DD1 4HN, United Kingdom*

³*Max Plank Institut für Quantenoptik, D-85740 Garching, Germany*

⁴*University of Essex, Colchester, CO4 3SQ, United Kingdom*

⁵*Laboratoire pour l'Utilisation des Lasers Intenses, Unité mixte CNRS-CEA-Ecole Polytechnique-Université Pierre et Marie Curie, Ecole Polytechnique, 91128 Palaiseau, France*

(Received 14 June 2000; published 29 March 2001)

The applicability of foams to equation of state experiments with laser-produced shocks has been studied. The pressure increase due to impedance mismatch at the payload-foam interface was measured experimentally using sub-ns laser pulses smoothed with phase zone plates. Foams of density in the range 5–900 mg/cm³ and of thicknesses of 50–150 μm were used. A model has been developed to study pressure amplification and the conditions under which the shock is stationary. Two-step two-material targets, allowing simultaneous measurements of the shock velocities in the two materials, were then used to obtain relative equation of state data. Pressures higher than 100 Mbar were achieved in gold.

DOI: 10.1103/PhysRevE.63.046410

PACS number(s): 52.50.Lp, 62.50.+p

I. INTRODUCTION

The study of the equations of state (EOS) of matter in high-pressure conditions (above 10 Mbar) is a subject of great interest for several fields of modern physics. In particular, it is important in the context of astrophysics and inertial confinement fusion research. Some EOS's already exist for this pressure range [1], but they mainly result from calculations and theoretical models, with only a few experimental data available to validate them; furthermore they exist for a restricted number of materials. Therefore, the behavior of many materials under high pressure is still unknown. In the past, EOS measurements in the tens of Mbar domain could be only performed by nuclear explosions. Nowadays it is possible to reach very high pressures in the laboratory by using powerful pulsed-laser-generated shock waves in solid material. Earlier experiments showed the possibility of producing shock waves with pressures up to 100 Mbar in a laser-irradiated solid [2,3], and in a target foil impacted by a laser-accelerated foil [4]. Pressures as high as 750 Mbar were achieved by using laser pulses of 25 kJ (at a wavelength $\lambda = 0.53 \mu\text{m}$) and a foil impact technique [5]. However, in many of these experiments the bad quality of shocks prevented them from being used as a quantitative tool in high-pressure physics.

The planarity and stationarity of the shock fronts, as well as the low preheating of the material ahead of the shock waves, are essential to obtain accurate measurements of the EOS. Recent experiments [6–8] proved the possibility of creating spatially very uniform shocks in solids either by using a direct-laser drive with optically smoothed laser beams or x-ray thermal radiation (indirect laser drive).

Once high quality shocks are obtained, it is possible to perform precise measurements of the shock parameters. In particular, EOS points can be obtained if two quantities of

the shocked material, related to the Hugoniot-Rankine relations [9], are measured simultaneously. In a recent experiment performed by Collins *et al.* [10], the simultaneous measurement of two parameters (the shock velocity D and the fluid velocity u) was applied to the measurement of the EOS of deuterium. The main problem connected with this method is that it is necessary to use high-energy laser pulses with the aim of maintaining a constant ablation pressure for a few nanoseconds, and of irradiating large target areas. Another method for the determination of EOS points is based on the impedance-matching technique, and consists of measuring the shock velocity simultaneously (on the same laser shot) in two different materials. This makes it possible to achieve a relative determination of one EOS point of one material by taking the EOS of another material as a reference. The reliability of this method, used in the past in nuclear experiments, was recently proven in laser-driven shock experiments [8,11], and applied to EOS measurements for Cu [12], doped plastics [13], low-density foams [14], and gold [15]. Such a method has the advantage that high pressures (10–50 Mbar) can be reached with lasers of relatively small size ($\approx 100 \text{ J}$).

However, the finite energy of the laser, combined with the request of having almost-one-dimensional shocks (and hence relatively large focal spots), fixes an upper limit to the pressure which can be obtained in the material. On the other hand, even if a very large system is available, the laser intensity on target cannot be increased indefinitely. Indeed, higher intensities mean a higher plasma temperature, and hence a larger x-ray generation in the corona. Also, above a certain intensity threshold, laser instabilities like stimulated raman scattering and two-plasmon decay [16] can take place in the plasma corona, bringing about an important production of hot electrons. Such nonlinear physical phenomena take place at laser intensities of the order of $10^{14}/\lambda^2 \text{ W/cm}^2$, where λ in μm is the laser wavelength. Since hard x rays and

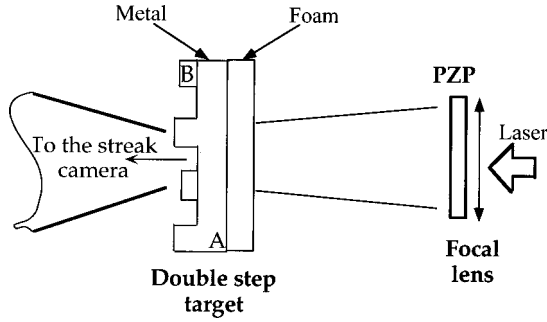


FIG. 1. Scheme of the experimental setup and target.

hot electrons are the principal causes of preheating of the material ahead of the shock wave, it is clear that intensities on target above this limit must be avoided in EOS experiments where target preheating is an unwanted and dangerous effect.

A practical way of reducing x-ray emission is the use of a low-Z ablator (e.g., plastic) before the target material. Luckily enough, this also proves to be a way to increase shock pressure due to the well-known impedance mismatch effect at the ablator-target interface [9]. (In passing, we note that the impedance-matching technique was used largely in the past to intensify laser-driven shock waves [17].)

In this paper, we study the possibility of maximizing such an effect by using low-density foams before the laser target. First we study the hydrodynamics of a layered foam-solid targets by analyzing the shock breakthrough from layered targets made of a foam layer on the laser side, and a stepped aluminum layer on the rear side. A streak camera is used to detect shock breakthrough at the base and at the step of the aluminum target, allowing the shock velocity to be determined. Since the EOS of aluminum is well known, we can thus determine the shock pressure.

We developed a simple analytical model to predict the shock pressure increment as a function of foam density and thickness. Such a model also addresses the question of shock stationarity, which is also essential to the use of laser-driven shocks for EOS measurements. Finally, we show the tentative application of the method to the measurement of one EOS point for gold.

II. EXPERIMENTAL TECHNIQUE AND SETUP

The experiment was performed using two different laser facilities (at MPQ and LULI) which could give different laser energies, and hence allowed different focal spots and laser intensities to be tested. First, we used the ASTERIX iodine laser at the MPQ, which delivers a single beam, of diameter 30 cm, with an energy of 250 J per pulse at a wavelength of $0.44 \mu\text{m}$. The temporal behavior of the laser pulse is Gaussian, with a full width at half maximum (FWHM) of 450 ps. Figure 1 shows the schematic experimental setup. The laser beam was focused directly onto the target with a $f=564 \text{ mm}$ lens. The primary condition of producing flat shock fronts imposed the use of the phase zone plate (PZP) [7,18] optical smoothing technique, in order to eliminate the large-scale spatial intensity modulations arising

from the coherent nature of the laser light, and to produce a flat-top intensity distribution in the focal spot. The design of this plate had Fresnel lenses of 2.5-cm diameter, which implies that 144 Fresnel lenses are covered by the laser beam. The characteristics of our optical system (PZP plus focusing lens) were such that we produced a total focal spot of $400\text{-}\mu\text{m}$ FWHM, with a $250\text{-}\mu\text{m}$ -wide flat region in the center corresponding to a laser intensity $I_L \approx 2 \times 10^{14} \text{ W/cm}^2$. Such large focal spots were needed in order to reduce two-dimensional effects, because the total thickness of the target could even be of the order of $170 \mu\text{m}$.

The diagnostic used to detect the shock emergence from the target rear face consisted of a $f=100 \text{ mm}$ objective imaging the rear face onto the slit of a streak camera, working in the visible region. The temporal resolution was better than 8 ps, and the imaging system magnification was $M=10$, allowing a spatial resolution better than $10 \mu\text{m}$. For what concerns the streak camera sweep speed, we considered an error of 1%, as suggested by the constructor. A protection system [19] was used for the diagnostics light path, to shield the streak camera from scattered laser light.

The second part of the experiment was realised at LULI. Three of the six beams of the LULI laser (converted into its second harmonic, $\lambda=0.53 \mu\text{m}$), with a total laser energy $E_{2\omega} \approx 100 \text{ J}$, were focused on the same focal spot. The temporal behavior of the laser pulse was Gaussian, with a FWHM of 600 ps. A fourth beam, also converted to 2ω , was used as a temporal fiducial. Each beam had a 90-mm diameter and was focused on target with an $f=500 \text{ mm}$ lens. The diagnostic system employed an objective (Olympus 50 mm, 1/1.2) used to image the target rear side onto the streak camera slit. Also, an active x-ray pinhole camera looking at the target on the laser side, at 22.5° with respect to the laser-beam plane, was used to check the plasma formation and to image the focal spot in the x-ray domain.

Phase zone plates were used too to produce a focal spot of $400\text{-}\mu\text{m}$ FWHM, with a $\approx 200\text{-}\mu\text{m}$ -wide flat region in the center, corresponding to a laser intensity $I_L \leq 6 \times 10^{13} \text{ W/cm}^2$. The shock emergence was also inferred by the emissivity of the target rear face, which was imaged by a photographic objective onto the slit of a visible streak camera with a 5-ps time resolution. We performed the calibration of the streak sweep speeds with an etalon made up with a series of short laser pulses (the FWHM is 100 ps). The relative error in the speed used for our experiments was lower than 1% [20]. The system magnification was $M=22$, allowing a $5\text{-}\mu\text{m}$ spatial resolution, which was checked by imaging a suitable grid.

III. TARGETS

In order to reduce one of the possible source of experimental errors, one needs high-quality, well-characterized targets with the structure presented in Fig. 1. In addition to an accurate knowledge of the step thicknesses, sharp step edges are required. Also, the spacing between the steps must be small compared to the flat portion of the focal spot, so that there is always at least one step in the spot region (as shown in Fig. 1), so to make the alignment easier.

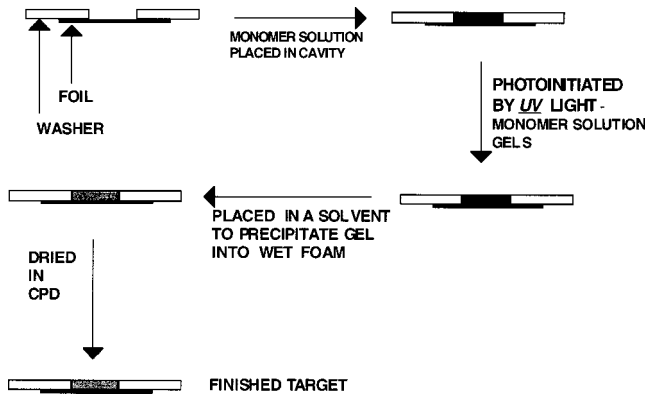


FIG. 2. Foam production.

Our targets were developed in collaboration with the ‘‘Laboratoire des cibles’’ of the Center d’Etudes de Limeil-Valenton [21]. The fabrication of the target, with an electron gun deposition technique, is made of three stages: first, the base material is deposited; a mask is then applied to this base in order to deposit the steps. Then a the foam layer is created, as explained in Sec. IV. For the Al/Au targets presented in the Sec. II, a second mask is applied, which is mechanically and optically guided, to ensure that the steps do not overlap and that their separation is limited to no more than $50\ \mu\text{m}$. The second step is then deposited (before the foam layer is created). The overall quality of the targets was checked by electron microscopy.

The aluminum base thickness was in the range of $10\text{--}18\ \mu\text{m}$, and the step in the range $4\text{--}6\ \mu\text{m}$. The Au step thickness was $2\text{--}3\ \mu\text{m}$. The step heights were determined with an absolute error equal to $0.03\ \mu\text{m}$. This ensured a relative error of about 1% for the aluminum step, and about 2% for the gold step.

IV. FOAM PRODUCTION

These targets were filled with the *in situ* polymerization techniques developed at Dundee university [22], summarized in Fig. 2. In this technique the targets are filled with a monomer solution containing a photoinitiator, and then polymerised *in situ* using UV light. The *in situ* polymerization technique produces foams in the required position in the target without the need for machining or handling, thereby reducing the risk of damage to the foam. Foams densities from $5\ \text{mg}/\text{cm}^3$ (or lower), to $900\ \text{mg}/\text{cm}^3$ can be produced by this technique, depending on the geometry of the target. The polymerization is a free radical process, and produces foams that are homogeneous with uniform submicron pore sizes.

The monomer used in the experiments described here was TMPTA (trimethylol propane triacrylate), the solution for polymerization was Brij® 30 [polyoxyethylene lauryl (4) ether], and the initiator was benzoin methyl ether. All of these chemicals were supplied by Aldrich Chemical Company. Brij® 30 was chosen as a solvent for polymerization to eliminate evaporation during the polymerization step. The small size of the targets makes the surface-to-volume ratio large, and therefore evaporation of the liquid in the targets becomes significant. The UV lamp used for polymerization

was an ORIEL Q 60000 lamp, equipped with a 100-W mercury lamp and a quartz fiber optic.

Targets were comprised of 50-, 100-, and $150\text{-}\mu\text{m}$ brass rings, closed at one end with three different types of films: (a) simple foil targets (gold or aluminum), or (b) foils with grid. These targets were filled with $5\text{--}200\text{-mg}/\text{cm}^3$ foams filled to the edge.

The targets were placed on a microscopic stage, and filled with a solution of monomer in Brij 30® using a syringe equipped with a microneedle (typically a $10\text{--}20\text{-}\mu\text{m}$ tip size). The targets were then illuminated with the UV light to polymerize the monomer in the Brij 30® solution. The solution gelled in a few seconds. These targets containing the gel were precipitated in a nonsolvent such as methanol. Once the precipitation of the gel was completed, they were dried with a critical point drying apparatus (Polaron 3100); see Fig. 2. Critical point drying is essential for the *in situ* polymerization technique. Any other drying method will damage the structure of the foam. Figure 3 shows electron microscope images of foam with different densities, showing a homogeneous structure in all cases.

V. EXPERIMENTAL RESULTS

Two streak camera images obtained at LULI are presented in Fig. 4. They show a shock breakout from targets with and without a foam layer. In both cases it is possible to see a time fiducial on the top right of the image, obtained by sending a portion of the laser beam onto the streak camera slit with an optical fiber. In the left image of Fig. 4(a), a stepped aluminum target without foam was used; while in the right image of Fig. 4(b), a foam layer was present on the laser side. All the other conditions, including the laser-pulse energy ($E_{2\omega} \approx 32\ \text{J}$), were the same.

Such pictures show a delayed shock breakthrough, i.e., a longer time between the maximum of the laser pulse (measured through the time fiducial) and shock arrival when the foam is present. This corresponds to the time needed for the shock to travel through the thick foam. The pictures also show that the shock velocity inside the aluminum target, and hence the pressure generated in aluminum, increases (the values of pressure have been deduced from shock velocity by using the SESAME tables [1]).

Such effects have been found to be a function of the foam density and thickness, as shown in the experimental results of Figs. 5 (LULI) and 6 (MPQ). While at LULI all targets had a $50\text{-}\mu\text{m}$ -thick foam layer and only density was changed, both parameters were varied during the MPQ experiment. The points corresponding to $\rho=1$ are those obtained with stepped targets without foam. The pressure generated in this last case (on average $\approx 18\ \text{Mbar}$ at MPQ and $\approx 8\ \text{Mbar}$ at LULI due to the reduced laser intensity) corresponds approximately to what can be obtained from scaling laws [23] for our laser and target parameters:

$$P \approx 8.6(I_L/10^{14})^{2/3} \lambda^{-2/3} (A/2Z)^{1/3}. \quad (1)$$

The points for $\rho = 1100\ \text{mg}/\text{cm}^3$ correspond to targets which have a layer of polymer at normal density. Here the plastic thickness is $15\ \mu\text{m}$ indeed the use of a $60\text{-}\mu\text{m}$ layer in this

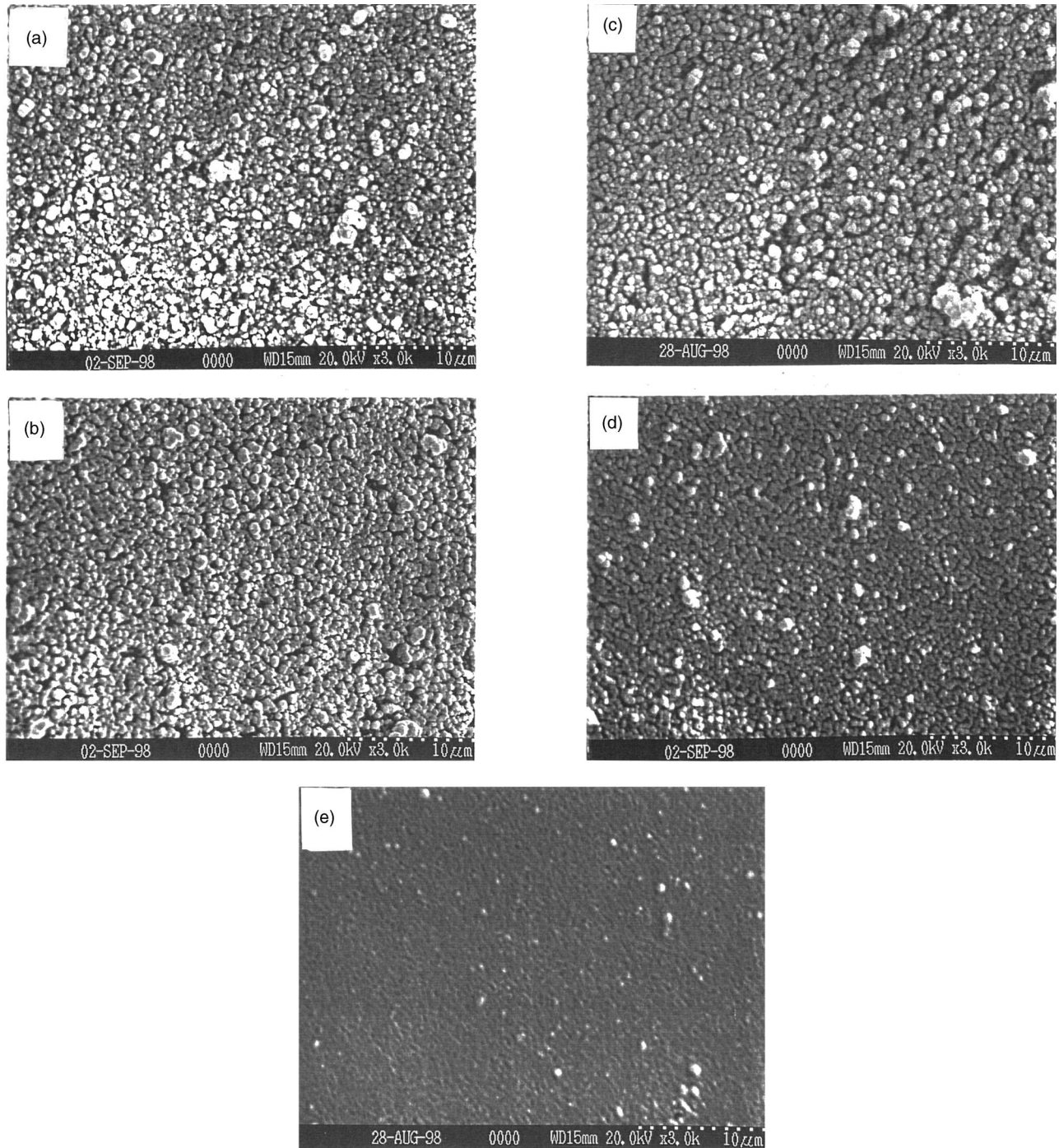


FIG. 3. Foams at different densities: (a) 50-mg/cm³ foam; (b) 100-mg/cm³ foam; (c) 200-mg/cm³ foam; (d) 400-mg/cm³ foam; and (e) 600-mg/cm³ foam.

case would have implied the shock pressure is not maintained, our laser pulse duration being too short (see Sec. VI).

Figures 7 and 8 show instead the delay of the shock arrival as a function of foam density. All of Figs. 5–8 also show the prediction obtained with the analytical model developed in Sec. VI.

The error bars of our points have been determined considering all the sources of errors in the measurement of D . The causes of possible errors are the uncertainties about the step thicknesses, the shock breakthrough time, and the streak

camera sweep speed. The cleanness of the signal (see Fig. 4) enabled us to obtain a precision of ± 4 psec in the shock breakthrough time. As stated in previous sections, the step heights of the targets have been measured with an absolute error of $0.03 \mu\text{m}$ and the streak camera sweep errors were $\leq 1\%$. With all the above errors taken into account, the shock velocities were determined with a maximum error of $\pm 5\%$ in aluminum. In deducing the error in the shock pressure, we took into account the relative error in the shock velocity, determined for each single shot. It is possible to show ex-

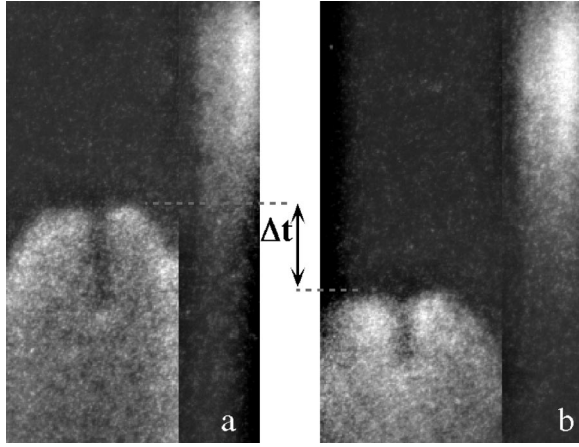


FIG. 4. Image of shock breakout obtained at LULI with a streak camera, without (left) and with (right) the foam layer. On the left we can observe a shot on a stepped aluminum target ($13 \mu\text{m}$, step $5 \mu\text{m}$). On the right we see the same target with a foam layer ($\rho = 50 \text{ mg/cm}^3$) on the laser side. The shock velocities were 18 km/s for a stepped aluminum target and 31 km/s for a target with a foam layer. The flat shock region is $\approx 200 \mu\text{m}$ large. The time delay Δt is 410 ps . The energy of the laser is $E_L \approx 32 \text{ J}$.

licitly that the relative error in the shock pressure is approximately double that of the shock velocity, in accordance with the quadratic dependence [9] between the two quantities.

VI. MODEL

The scope of this section is to develop a simple model to describe the behavior of the shock pressure in the foam and in the metal vs time and check the stationarity of the shock in the foam and in the metal as a function of foam thickness and density. We recall that, within some assumptions to be

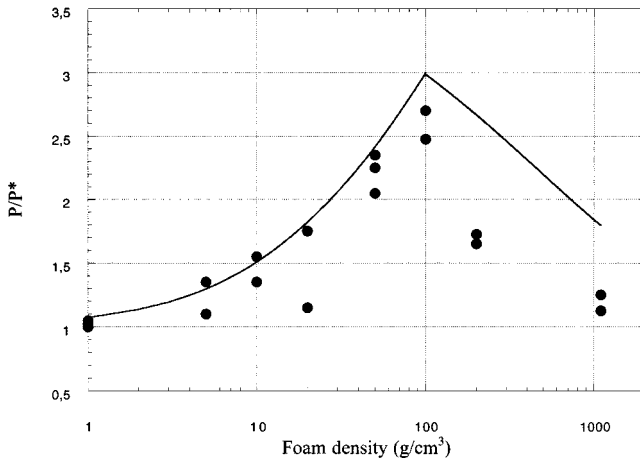


FIG. 5. Experimental results P/P^* vs the foam density ρ , interpolated by Eqs. (9) and (14). Points obtained in the LULI experiment. The solid curve represents the pressure $P_{\text{eff}}/P^* = [1 + (P/P^*)^2]^{1/2}$, where P is obtained from Eq. (9) when $\rho < \rho_C$, or from Eq. (14) when $\rho > \rho_C$. P^* is the ablation pressure (8 Mbar in this case), and the critical density is $\rho_C \approx 100 \text{ mg/cm}^3$.

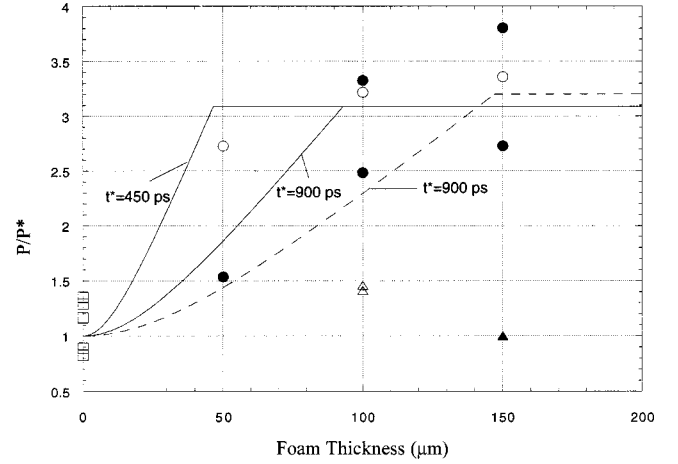


FIG. 6. Experimental results P/P^* vs the foam thickness d , interpolated by Eqs. (9) and (14). Solid curve represents $P_{\text{eff}}/P^* = [1 + (P/P^*)^2]^{1/2}$, with the ablation pressure $P^* = 18 \text{ Mbar}$. Points are obtained in the MPQ experiment: full circles: foam layer (density 20 mg/cm^3) plus Au layer ($6.9 \mu\text{m}$); empty circles: foam layer (density 50 mg/cm^3) plus Au layer ($6.9 \mu\text{m}$); empty triangles: foam layer (density 50 mg/cm^3) plus Al layer ($24.4 \mu\text{m}$); full triangles: foam layer (density 100 mg/cm^3) plus Al layer ($24.4 \mu\text{m}$); squares: points obtained in a metal layer without foam. The interpolations shown (obtained using $t^* = 900 \text{ ps} = 2t_L$) refer to points obtained in targets composed of a foam layer (density 20 mg/cm^3) and Au layer ($6.9 \mu\text{m}$) (dashed curve) and points obtained in targets composed of a foam layer (density 50 mg/cm^3) and an Au layer ($6.9 \mu\text{m}$) (solid curve). In this case we also show, for comparison, the curve obtained using $t^* = 450 \text{ ps} = t_L$, which provides a worse fit to the experimental data.

discussed later, shock velocity may be related to the shock pressure by

$$D_{\text{max}} = \left(\frac{(\gamma + 1) P^*}{2 \rho_1^0} \right)^{1/2}, \quad (2)$$

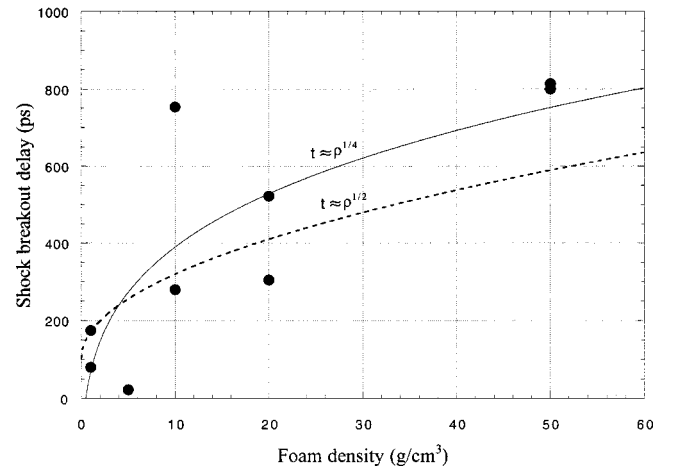


FIG. 7. Shock breakthrough delay vs foam density. Experimental data are obtained from the LULI experiment, and are compared to quadratic (solid lines) and quartic [dashed lines, Eq. (13)] scaling laws.

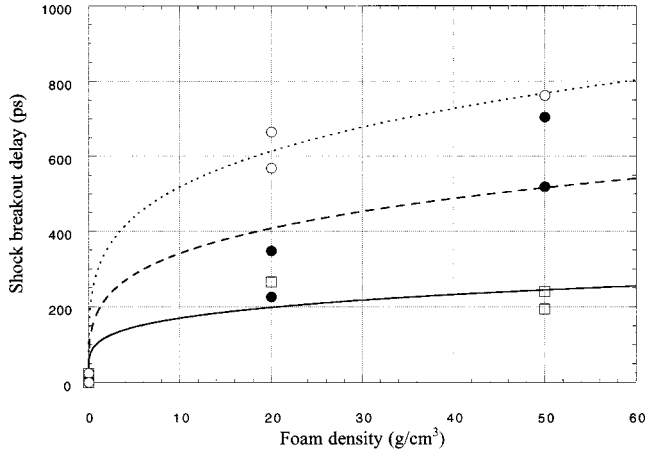


FIG. 8. Shock breakthrough delay vs foam density. Experimental data are obtained from the MPQ experiment, and are compared to quartic [Eq. (13)] scaling laws. Squares refer to targets with a 50- μm foam layer (interpolated by the solid curve), full circles to those with a 100- μm foam layer (interpolated by the dashed curve), and empty circles to those with a 150- μm foam layer (interpolated by the dotted curve).

where P^* is the pressure generated by the laser in the foam and given by Eq. (1).

We observe that P^* depends only very weakly on the target material but strongly on the laser parameters. Since the laser intensity changes with time, we can assume that the shock speed and the shock pressure undergo a first phase in which they increase (acceleration phase, $t < t^*$), remain constant in a second phase (corresponding to the maximum of the laser pulse), and decrease in a third phase, due to bidimensional effects in shock propagation and the damping of the laser pulse.

In the acceleration phase of the shock, $t < t^*$, we can simply assume a linear increase of the shock speed, and write

$$D = D_{\max} \frac{t}{t^*}. \quad (3)$$

Therefore the shock acceleration is

$$a = \frac{dD}{dt} \equiv \frac{D_{\max}}{t^*}. \quad (4)$$

Since the shock speed and the shock pressure achieve a constant value after a phase of acceleration, the shock can reach an interface between the foam and the metal (gold or aluminum, in our experiments) before it has reached its maximum value. In this case, the shock pressure will continue to increase in the metal and hence stationarity will not be achieved in the all metal thickness.

On the other side, at late times, the shock may be nonstationary due to the relaxation in the material. This may be originated at the end of the laser pulse, but it may take place before due to the following mechanism. When the shock reaches the foam-metal interface, the pressure of the transmitted shock increases due to the impedance mismatch effect [9] since the metal mass density is much bigger than the

foam density. At the same time a shock with equal pressure will be reflected in the foam (the foam metal interface being in dynamical equilibrium, i.e., the pressure on the two sides being the same). The reflected shock will travel back in the foam until it reaches the critical surface. Here the laser can only sustain a pressure equal to the ablation pressure [Eq. (1)]. The difference between these two pressures will generate an unloading wave that runs rapidly in the foam and in the metal and may eventually reach the shock transmitted in the metal before it emerges from target rear side. This can reduce the shock pressure in the target, so that the shock will no longer be stationary.

Hence the shock may be nonstationary in the metal, either because the foam is too thin or tenuous (and the shock arrives at the interface while it is still in the acceleration phase) or because it is too thick or dense (and the unloading wave has the time to reach the shock before its breakout from the target rear side). We will now discuss separately all these issues.

A. Nonstationarity at early times

Let us discuss the first problem. The laser strikes the foam, and generates a shock wave with pressure P_1 , that propagates in the foam with speed D_1 . When it arrives at the foam-metal interface, a shock will be transmitted, and another one will be reflected in the foam: both will have the same pressure P_2 ($P_2 > P_1$), but the shock velocities will be different (D_2 and D_3 , respectively). We now consider the following simplifying assumptions.

(1) We use the equation of state of perfect gas both for the foam and the metal, that is,

$$E = \frac{1}{\gamma - 1} PV,$$

where E represents the energy per mass unit.

(2) The reflected shock is represented, in the (u, P) plane, by the curve symmetrical to the foam shock polar crossing the point (u_1, P_1) (see Fig. 9) [9].

The first hypothesis, combined with the Hugoniot-Rankine relations, allows one to obtain

$$P = \frac{\gamma + 1}{2} \rho_0 u^2, \quad (5)$$

$$P = \frac{2}{\gamma + 1} \rho_0 D^2. \quad (6)$$

The factor γ for a monatomic perfect gas is 5/3. Here, in order to obtain a more realistic description of the compressed metal, we have used a value of γ which is obtained by fitting Eq. (5) to the shock polar given by the SESAME tables for Al and to that given in Ref. [24] for Au (indeed measurements reported in Ref. [15] suggested that SESAME is not correct for gold at high pressures). Hence we obtain $\gamma_{\text{Al}} = 1.64$ and $\gamma_{\text{Au}} = 2.25$, and in the following $\gamma_{\text{foam}} = \gamma$ will be different from that of the metal γ_m .

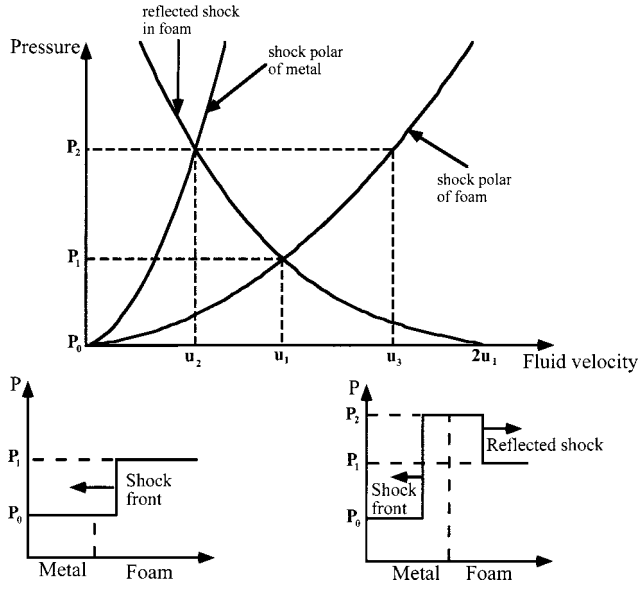


FIG. 9. Representation of the impedance mismatch principle. On the bottom, we show shock fronts in the metal and in the foam before and after the shock reaches the interface.

The second hypothesis allows one to define the material velocity u_2 behind reflected and transmitted shocks: observing that the vertex of the reflected polar lies in the point $(2u_1, P_0)$, and referring to Fig. 9, we can write

$$u_2 = 2u_1 - u_3. \quad (7)$$

Using these relations, and following the approach used in Refs. [25], [26], we arrive to the following equations for D_2 and P_2 :

$$D_2 = \frac{(2P_1)^{1/2}(\gamma+1)^{1/2}(\gamma_m+1)^{1/2}}{(\gamma_m+1)^{1/2}(\rho_1^0)^{1/2} + (\gamma+1)^{1/2}(\rho_2^0)^{1/2}}. \quad (8)$$

The symbols ρ_1^0 and ρ_2^0 indicate the unperturbed foam and metal density, respectively.

If the shock reaches the interface when it is already stationary then $P_1 = P^*$, as given by Eq. (1), and then we obtain an expression for the scaling of shock pressure in the metal vs foam density:

$$P_2 = \frac{4\rho_2^0 P^* (\gamma+1)}{[(\gamma_m+1)^{1/2}(\rho_1^0)^{1/2} + (\gamma+1)^{1/2}(\rho_2^0)^{1/2}]^2}. \quad (9)$$

Within our simplifying assumptions, this is the analytical expression of the impedance mismatch principle. Decreasing the foam density the mismatch between the two materials increases, while the ablation pressure P^* is independent on density. Hence higher and higher pressures are reached in the metal.

Our experimental data clearly show that such a trend is reversed below a certain foam density (or a given thickness). This is explained by the fact that in this case the shock reaches the foam-metal interface before t^* , i.e., before the pressure has reached its maximum value P^* .

The characteristics of the laser pulse and the foam (thickness and density) determine the time t_a employed by the shock to go through the foam. If $t_1 < t^*$, then the thickness of the foam and t_a are related through the relation

$$d_{\text{foam}} = \frac{1}{2} a t_a^2.$$

Recalling Eqs. (3) and (4), we obtain the value of D_1 ,

$$D_1 = \left(\frac{2d_{\text{foam}} D_{\text{max}}}{t^*} \right)^{1/2},$$

which, combined with Eqs. (2) and (6), yields

$$P_1 = \left(\frac{2d_{\text{foam}}}{t^*} \right) \left(\frac{2\rho_1^0 P^*}{\gamma+1} \right)^{1/2}. \quad (10)$$

We note that in the limiting case $t_a = t^*$, we of course obtain $D_1 = D_{\text{max}}$ and $P_1 = P^*$.

The shock pressure at the interface, therefore, depends on the foam thickness and on the foam density (in different ways). Fixing the foam thickness, and substituting in Eq. (8) the value obtained for P_1 using Eq. (10), we obtain

$$D_2 = \frac{2(\gamma+1)^{1/2}(\gamma_m+1)^{1/2}}{(\gamma_m+1)^{1/2}(\rho_1^0)^{1/2} + (\gamma+1)^{1/2}(\rho_2^0)^{1/2}} \times \left(\frac{d_{\text{foam}}}{t^*} \right)^{1/2} \left(\frac{2\rho_1^0 P^*}{\gamma+1} \right)^{1/4}.$$

In a similar way, we can obtain an explicit expression for the shock pressure in the metal:

$$P_2 = \frac{8\rho_2^0 (\gamma+1)^{1/2} (2\rho_1^0 P^*)^{1/2}}{[(\gamma_m+1)^{1/2}(\rho_1^0)^{1/2} + (\gamma+1)^{1/2}(\rho_2^0)^{1/2}]^2} \frac{d_{\text{foam}}}{t^*}. \quad (11)$$

This equation describes the shock pressure in the metal layer when the shock arrives at the interface before it has reached its maximum. We see that, in this case, P_2 increases with the foam density ρ_1^0 approximately as $(\rho_1^0)^{1/2}$.

We can express this condition as a function of the foam density. From Eq. (10) we can observe that $P_1 = P^*$ for a particular density value, which we will call the critical density ρ_c . This density value is then given by

$$P^* = P_1 = \left(\frac{2d_{\text{foam}}}{t^*} \right) \left(\frac{2\rho_1^0 P^*}{\gamma+1} \right)^{1/2},$$

and, therefore,

$$\rho_c = \frac{(\gamma+1)(t^*)^2}{2^3 d_{\text{foam}}^2} P^*. \quad (12)$$

In conclusion, in this section, we have obtained the following relations between the shock pressure in the metal layer and the density: If $\rho < \rho_c$ (or $t_1 < t^*$),

$$\frac{P_2}{P^*} = \frac{8\rho_2^0 (\gamma+1)^{1/2} (2\rho_1^0 / P^*)^{1/2}}{[(\gamma_m+1)^{1/2}(\rho_1^0)^{1/2} + (\gamma+1)^{1/2}(\rho_2^0)^{1/2}]^2} \frac{d_{\text{foam}}}{t^*};$$

and, if $\rho > \rho_C$ (or $t_1 > t^*$),

$$\frac{P_2}{P^*} = \frac{4\rho_2^0(\gamma+1)}{[(\gamma_m+1)^{1/2}(\rho_1^0)^{1/2} + (\gamma+1)^{1/2}(\rho_2^0)^{1/2}]^2}.$$

B. Shock transit time

Let us now discuss the relation between the time employed by the shock to go through the foam and the foam density: in Figs. 7 and 8 we show the experimental data compared with the theoretical curves (in the density range $\rho < \rho_C$). Times here are the delays measured when foam is present on the target (that is to say that $t=0$ corresponds to the shock arrival time in a target without foam). If we consider the shock velocity constant while the shock goes through the foam, the time t_a employed by the shock to go through the foam should be written as

$$t_a = \frac{d_{\text{foam}}}{D},$$

where d_{foam} is the foam thickness and D the shock velocity in the foam. Using Eq. (2), we obtain that t_a scales as $\rho^{1/2}$. However, our experimental points to the density interval $\rho < \rho_C$, and the shock velocity is not constant in the foam undergoing an acceleration phase. We can therefore write d_{foam} as

$$d_{\text{foam}} = \frac{1}{2} a t^2.$$

For t_a , we can use relation (5) to obtain

$$d_{\text{foam}} = \frac{1}{2} \frac{D_{\text{max}}}{t^*} t_a^2,$$

and, therefore,

$$t_a^2 = \frac{2t^* d_{\text{foam}}}{D_{\text{max}}}.$$

Now, using relation (2) for D_{max} , we obtain

$$t_a = \left(\frac{2t^* d_{\text{foam}}}{\left(\frac{\gamma+1}{2} P^* \right)^{1/2}} \right)^{1/2} \rho^{1/4}. \quad (13)$$

Hence, in the acceleration phase, the arrival time scales as $\rho^{1/4}$ (see Sec. VI E for a comparison with experimental data).

C. Very tenuous foams

The trend $P_2 \approx (\rho_1^0)^{1/2}$ for $\rho < \rho_C$ continues down to a value of ρ_1^0 for which the plasma generated in the foam becomes undercritical, and hence transparent to laser light. If we assume a complete ionization of the low- Z elements of the foam, this happens when

$$n_e = \rho N_A Z/A < n_c = 1.1 \times 10^{21}/\lambda^2,$$

where N_A is the Avogadro number. This fixes a limit at $\rho \approx 12 \text{ mg cm}^{-3}$ (for $\lambda = 0.53 \text{ } \mu\text{m}$). A partial ionization is not likely, considering the high temperatures reached in the foam (as shown in numerical simulations), but this would mean that an even higher foam density is required to reach the critical density.

Also, at the lowest densities, it is not possible to avoid a direct interaction of the laser beam with the metal target behind the foam due to the fast ablation rate of the foam. Simple analytical laws predict the ablation rate [27] to be

$$\begin{aligned} \dot{m} (\text{kg/cm}^2 \text{ s}) &= 4.5 \times 10^{-6} [I (\text{W/cm}^2)]^{3/4} \\ &\times [\lambda (\mu\text{m})]^{-1/2} [t (\text{ns})]^{-1/4}. \end{aligned}$$

Hence the ablation rate (and the shock pressure) is independent of the foam density, and the ablation velocity is inversely proportional to it, giving, in the case of laser parameters used at LULI, a limit of about $\rho \approx 15 \text{ mg cm}^{-3}$. Foams with lower density are completely ablated during the pulse.

These two effects contribute to gradually lowering the shock pressure to the value measured in simple metal targets, hence producing the expected continuity of physical results. The residual measured pressure increment for such low densities is probably due to the partial confinement of the expanding aluminum plasma by the foam, as observed in shocks produced from focusing lasers on the surface of targets immersed in water or under a layer of transparent material [28].

In the limiting case when no foam is present ($\rho_1^0 = 0$ or $d = 0$), we must of course obtain a shock pressure $= P^*$ in the metal. Hence, in order to obtain a simple analytical expression for the shock pressure P_1 valid for all foam densities $\rho < \rho_C$, we assumed

$$P_2^{\text{eff}} = \sqrt{P^{*2} + P_2^2} \quad (14)$$

for the shock pressure in the metal, where P_2 is given by Eq. (11) (see Sec. VI E for a comparison with experimental data).

D. Late times, thick foams, role of relaxation wave

Now we will discuss the second stationarity criterion for shock in the metal. As already observed, when the reflected shock in the foam reaches the critical surface, an unloading wave is generated. If this wave reaches the shock wave before it has reached the target rearside, the shock will not be stationary, and the shock pressure will be reduced. This process is shown in Fig. 10.

If the shock reaches the interface when it is already stationary, it will require a time $t_1 = D_2/d_{\text{met}}$ to arrive at the target rearside. Now we calculate the sum of the following intervals.

(i) The time $t_{1\text{foam}}$ needed to the reflected shock to go through the foam, considering that the foam is compressed (and therefore its thickness is reduced).

(ii) The time $t_{2\text{foam}}$ needed for the unloading wave generated at the critical surface to go through the compressed

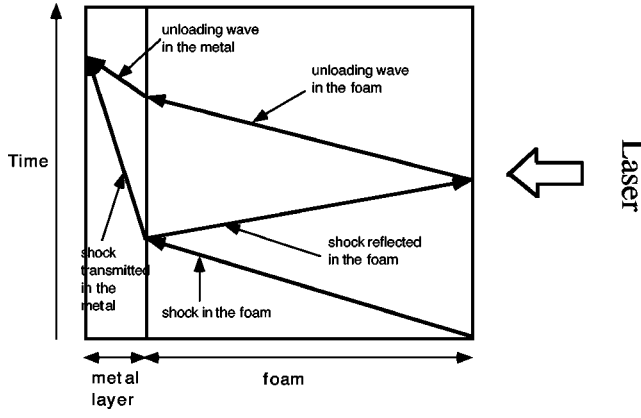


FIG. 10. Dynamics of shock and relaxation waves in a two-layer target.

foam two times (first by direct shock and then by the reflected shock): this wave propagates at the sound velocity c_s .

(iii) The time t_2 needed for the unloading wave to go through the compressed metal.

If $t_{1\text{foam}} + t_{2\text{foam}} + t_2$ is less than t_1 , the unloading wave reaches the shock wave before it has emerged from the rear-side of the target, and the shock will not be stationary. To calculate $t_{1\text{foam}}$ we have to determine the speed of the reflected shock. This is possible using Eq. (6), valid for a perfect gas, and assuming a density $\rho \approx 4\rho_1^0$, because the density of a perfect gas compressed by a very strong shock is increased by a factor 4. The speed of the reflected shock is therefore

$$D_3 = \left(\frac{\gamma + 1}{2} \frac{P_2}{4\rho_1^0} \right)^{1/2}. \quad (15)$$

The time employed by the reflected shock to go through the foam is then easily calculable, but it is important to observe that the thickness has been reduced to $d_{\text{foam}}/4$ because of the foam compression by the direct shock. Hence

$$t_{1\text{foam}} = \frac{d_{\text{foam}}}{4D_3}. \quad (16)$$

At the critical surface an unloading wave is generated, which travels through the target with the sound velocity in the compressed foam:

$$c_s = \left(\gamma \frac{P_2}{\rho_1} \right)^{1/2}. \quad (17)$$

P_2 is the pressure of the reflected shock, $\rho_1 = 16\rho_1^0$ (the foam has undergone the passage of two shocks, and compressed two times of a factor 4).

Also the foam thickness is now $d_{\text{foam}}/16$. Hence

$$t_{2\text{foam}} = \frac{d_{\text{foam}}}{16c_s}. \quad (18)$$

TABLE I. Parameters calculated by applying the model described in Sec. VID to verify the shock stationarity.

	Al	Au
P_2	55.85 Mbar	64.54 Mbar
t_1 (experimental)	467 ps	296 ps
D_3 foam [Eq. (15)]	192.96 km/s	207.43 km/s
$t_{1\text{foam}}$ [Eq. (16)]	130 ps	120 ps
c_s foam [Eq. (17)]	107.87 km/s	115.96 km/s
$t_{2\text{foam}}$ [Eq. (18)]	58 ps	54 ps
c_s met [Eq. (19)]	29.12 km/s	13.71 km/s
t_2 [Eq. (20)]	209 ps	126 ps
$t_{1\text{foam}} + t_{2\text{foam}} + t_2$	397 ps	300 ps

Finally, the unloading wave has to travel through the metal layer, where the density has increased about four times and thickness has been reduced about four times by the direct shock (the metal behavior is less close to a perfect gas than that of foams, so this is a worse approximation). The sound velocity in the metal layer is

$$c_{s\text{met}} = \left(\gamma_{\text{met}} \frac{P_2}{4\rho_2} \right)^{1/2}, \quad (19)$$

and the time required by the unloading wave to go through the metal layer compressed by shock is

$$t_{2\text{met}} = \frac{d_{\text{met}}}{4c_{s\text{met}}}. \quad (20)$$

E. Comparison with experimental data

In this section we will compare the experimental data with the models developed in the previous sections. Figure 5 shows the experimental data for P/P^* vs foam density obtained at LULI, and their interpolation using Eqs. (9) and (14). It is evident that in this case $\rho_C \approx 100 \text{ mg/cm}^3$. The ablation pressure P^* was about 8 Mbar at LULI and about 18 Mbar at MPQ, both in Al and Au targets. This was measured using step targets without a foam layer, and resulted in agreement with the value given by Eq. 1. Also, to draw the interpolation we have used $t^* - t_0 = 2\tau$, where τ is the FWHM duration of the laser pulse. This implies $(t^* - t_0) = 900 \text{ ps}$ for the MPQ experiment and 1200 ps for the LULI experiment. This choice gave the best agreement between our analytical model and the predictions of computer simulations [25,26].

Figure 6 shows the results obtained at MPQ. Here they have been represented as functions of the foam thickness, making it clear that, for very thin foams, shock stationarity has not been obtained. While Fig. 6 shows a fair agreement between experimental results and model prediction for gold, the situation is completely different for Al. This is due to the relaxation wave. Indeed, let us consider the case of a 50-mg/cm^3 foam layer and a metal layer with a thickness of $6.9 \mu\text{m}$ for Au and one of $24.4 \mu\text{m}$ for Al.

In Table I we report all the results obtained using the

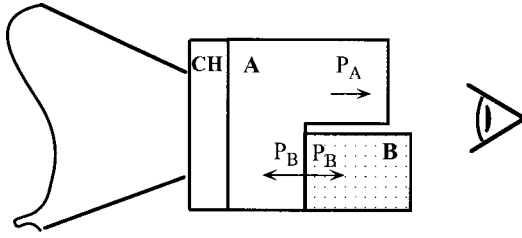


FIG. 11. Principle of two-step–two-material targets.

model presented in Sec. VID (equations used to calculate these values are also indicated in Table I). The pressure P_2 of the reflected and transmitted shock is calculated using Eq. (9), where ρ_1^0 is the foam density, ρ_2^0 is the metal density (2.7 g/cm³ for Al and 19.3 g/cm³ for Au).

We can observe that in the aluminum case the unloading wave reaches the shock wave before it arrives at the rear side of the target; then the shock is nonstationary in the case of Al, which explains the behavior of Al experimental points in Fig. 6. Finally, Figs. 7 and 8 show the experimental behavior of the shock arrival time as a function of the foam density. Results have been interpolated with the function

$$t_a = a\rho^{1/4}$$

[see Sec. VIE and Eq. (13)]. In Fig. 7, we also represent the interpolation $t_a = a\rho^{1/2}$ which is obtained if we consider D to be constant.

VII. Application to EOS experiments

In Sec. VI, we used foams in a preliminary experiment for the measurement of the EOS of gold. Such an EOS experiment is based on the impedance-matching technique [9] applied to a two-step, two-material target, with the structure sketched in Fig. 11. The target is made of a base of a material A (reference material), which supports two steps, one of the same material A and the other one of a material B (the material to be investigated). The target side, corresponding to the base, was irradiated with the laser so that, recording the temporal evolution of the rear face emissivity, it was possible to measure the shock breakout time from the base and from the steps. Therefore, this target geometry allows the shock velocities D_A and D_B to be experimentally determined in the two materials on the same laser shot. By knowing the EOS of material A and using impedance-matching conditions [9], we could then find the EOS points of material B. Here the reference material was aluminum which has a well known EOS [1] in the investigated pressure range, and material B was gold.

Figure 12 shows a typical streak image of a two-step target obtained at MPQ. Due to the large target thickness, two-dimensional effects are already quite appreciable, giving a curved shock breakout. However the central part ($\geq 100 \mu\text{m}$) is still flat enough to allow the measurement and a comparison of the shock velocities in the two materials.

Here the experimental aluminum shock velocity is $D_A \approx 48.17 \mu\text{m/ns}$, corresponding to $P \approx 45.29 \text{ Mbar}$, and the gold shock velocity is $D_B \approx 28.64 \mu\text{m/ns}$. The corresponding

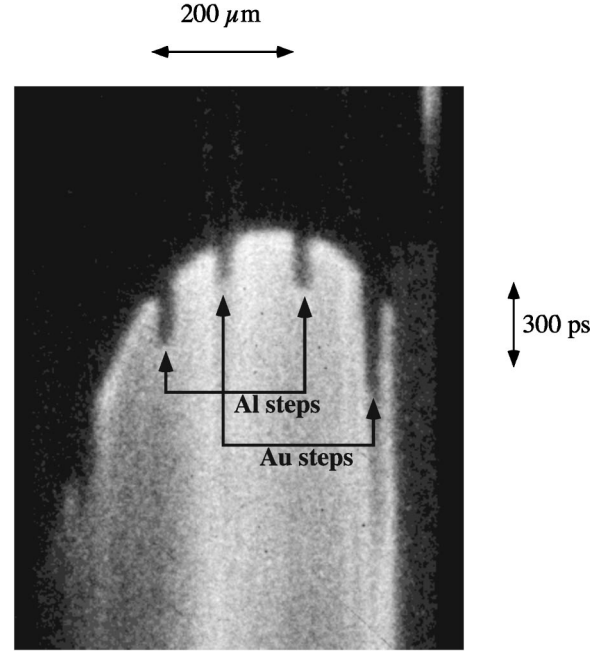


FIG. 12. Experiment on a double-step target: streak camera record of visible light emitted by the rear side of the target. The target consists of a base of aluminum (thickness $18 \mu\text{m}$) and two steps of gold ($2.87 \mu\text{m}$) and aluminum ($6.4 \mu\text{m}$), respectively.

pressure and fluid velocity, found by impedance mismatch, in gold are 108.1 Mbar and 19.56 km/s, in fair agreement with the scaling given in Ref. [24] (which would give $P = 95.84 \text{ Mbar}$ and $u = 17.34 \text{ km/s}$ when $D = 28.64 \text{ km/s}$). This is in fair agreement with recent data published on gold shock compression [15].

VIII. CONCLUSIONS

In this paper we have discussed the applicability of foams as pressure amplifiers in EOS experiments with laser-produced shocks. The pressure increase due to impedance mismatch at the payload-foam interface was measured experimentally using sub-ns laser pulses smoothed with phase zone plates. Foams of densities $\geq 5 \text{ mg/cm}^3$ and thickness $\geq 50 \mu\text{m}$ were used. A model has been developed to study pressure amplification and the conditions under which the shock is stationary. Two-step, two-material targets, allowing the simultaneous measurements of the shock velocities in the two materials, were then used to obtain relative equation of state data. Pressures higher than 100 Mbar were achieved in gold.

Increments of a factor ≥ 3 in shock pressure have been demonstrated. Due to the weak scaling of pressure vs laser intensity [see Eq. (1)], this would require a factor ≈ 6 increment in intensity on target for which a kJ laser would be necessary. Also, this would imply the use of intensities falling in the nonlinear regime, where preheating can become quite dangerous.

Our results may open the way to the use of foams in EOS experiments such those described in Ref. [15]. In this case the use of foams can be a relatively easy way of relaxing laser energy requirements. Hence foams can increase the efficiency of direct drive EOS experiments (already more effi-

cient than x-ray indirect drive [12]), allowing very high pressures to be reached with relatively small laser systems.

ACKNOWLEDGMENTS

This work was supported by E.U. HCM and TMR programmes under Contract Nos. CHRX-CT93-0377, CHRX-

CT93-0338, and ERB-CH-CT92-0006. We would like to thank Ian Ross and Colin Danson of Rutherford Appleton Laboratory, for helpful discussions on the PZP technique and for calculations concerning the PZP design. We thank Stefano Atzeni for the useful discussion on the analytical model. Finally we warmly acknowledge the support of the MPQ and LULI technical teams during the experiments.

-
- [1] *T-4 Handbook of Material Properties Data Bases, Vol. 1c: Equations of State*, edited by K. S. Holian, LANL Report No. LA-10160-MS, UC-34, November 1984; B. I. Bennett *et al.*, LANL Report No. LA-7130 (1978); *SESAME Report on the Los Alamos Equation-of-State Library*, Report No. LALP-83-4 (T4 Group LANL, Los Alamos, 1983).
- [2] C. G. M. van Kessel and R. Sigel, *Phys. Rev. Lett.* **33**, 1020 (1974); L. R. Veerer and S. C. Solem, *ibid.* **40**, 1391 (1978); R. J. Trainor *et al.*, *ibid.* **42**, 1154 (1978); F. Cottet *et al.*, *ibid.* **52**, 1884 (1984); J. D. Kilkenny, University of California Report No. UCRL 50021-86, 1987, pp. 3–6.
- [3] F. Cottet *et al.*, *Appl. Phys. Lett.* **47**, 678 (1985).
- [4] R. Fabbro *et al.*, *Laser Part. Beams* **4**, 413 (1986); S. P. Obenschain *et al.*, *Phys. Rev. Lett.* **50**, 44 (1983); B. Faral *et al.*, *Phys. Fluids B* **2**, 371 (1990).
- [5] R. Cauble *et al.*, *Phys. Rev. Lett.* **70**, 2102 (1993).
- [6] Th. Löwer *et al.*, *Phys. Rev. Lett.* **72**, 3186 (1994).
- [7] M. Koenig *et al.*, *Phys. Rev. E* **50**, R3314 (1994).
- [8] D. Batani, S. Bossi, A. Benuzzi, M. Koenig, B. Faral, J. M. Boudenne, N. Grandjouan, S. Atzeni, and M. Temporal, *Laser Part. Beams* **14**, 211 (1996).
- [9] Ya. B. Zeldovich and Yu. P. Raizer, *Physics of Shock Waves and High Temperature Hydrodynamic Phenomena* (Academic, New York, 1967).
- [10] G. W. Collins *et al.*, *Science* **281**, 1178 (1998).
- [11] M. Koenig *et al.*, *Phys. Rev. Lett.* **74**, 2260 (1995).
- [12] A. Benuzzi *et al.*, *Phys. Rev. E* **55**, R6356 (1996).
- [13] B. Faral, M. Koenig, J. M. Boudenne, D. Batani, A. Benuzzi, S. Bossi, M. Temporal, S. Atzeni, and Th. Löwer, in *High Pressure Science and Technology* (AIP, New York, 1996), p. 943.
- [14] M. Koenig, A. Benuzzi, F. Philippe, D. Batani, T. Hall, N. Grandjouan, and W. Nazarov, *Phys. Plasmas* **6**, 3296 (1999).
- [15] D. Batani *et al.*, *Phys. Rev. B* **61**, 9287 (2000).
- [16] H. A. Baldis, E. M. Campbell, and W. L. Krueer, in *Handbook of Plasma Physics*, edited by M. N. Rosenbluth and R. Z. Sagdeev (North-Holland, Amsterdam, 1991), Vol. 3, Chap. 9.
- [17] R. Fabbro *et al.*, *Laser Part. Beams* **4**, 413 (1986); S. P. Obenschain *et al.*, *Phys. Rev. Lett.* **50**, 44 (1983); B. Faral *et al.*, *Phys. Fluids B* **2**, 371 (1990).
- [18] R. M. Stevenson *et al.*, *Opt. Lett.* **19**, 363 (1994).
- [19] Th. Löwer and R. Sigel, *Contrib. Plasma Phys.* **33**, 355 (1993); and in *High Pressure Science and Technology* (Ref. [13]), p. 1261.
- [20] A. Benuzzi *et al.*, *Rapport Scientifique LULI 1995* (1996), p. 289.
- [21] B. Faral *et al.*, *Rapport Scientifique LULI 1993* (1994), p. 309.
- [22] J. Falconer *et al.*, *J. Vac. Sci. Technol. A* **13**, 1941 (1995); **12**, 2798 (1994).
- [23] J. Lindl, *Phys. Plasmas* **2**, 3933 (1995).
- [24] L. V. Al'tshuler, K. K. Krupnikov, and M. I. Brazhnik, *Zh. Eksp. Teor. Fiz.* **7**, 7 (1958) [*Sov. Phys. JETP* **34**, 4 (1958)].
- [25] W. Nazarov, D. Batani, A. Masini, A. Benuzzi, M. Koenig, B. Faral, T. Hall, and Th. Löwer, *Laser Part. Beams* **17**, 3 (1999); **17**, 529 (1999).
- [26] M. Temporal, S. Atzeni, D. Batani, and M. Koenig, *Eur. Phys. J. D* **12**, 509 (2000).
- [27] P. Mora, *Phys. Fluids* **25**, 1051 (1982).
- [28] R. Fabbro *et al.*, *J. Appl. Phys.* **68**, 775 (1990).